Modeling the annealing of dislocation loops in implanted c-Si solar cells

F. A. Wolf, A. Martinez-Limia, D. Stichtenoth, and P. Pichler, *Senior Member, IEEE*

***Abstract*—This paper is motivated by the question of how residual implantation damage degrades solar cell performance. In order to avoid such degradation, annealing processes of implanted c-Si solar cells use high thermal budgets. Still, implantation-induced dislocation loops may survive these processes. We derive two models for the annealing kinetics of dislocation loops that are suitable for the study of high thermal budgets: A model that is able to describe the parallel ripening of faulted and perfect dislocation loops, and a model that explicitly implements the conservative and non-conservative processes associated with Ostwald ripening. Both models lead to better agreement with experiment than what has been published before.**

I. Introduction

STUDIES of implanted solar cells carried out within recent years showed that significantly higher thermal budgets than in microelectronics are needed to achieve satisfactory cell performance [1, 2, 3, 4]. Typically, for such annealing conditions ($> 950\,^{\circ}\mathrm{C}$, $> 10\,\mathrm{min}$), the primary implant damage evolves into a defect configuration in which only dislocation loops survive. Such loops were found to correlate with the emitter saturation current [5, 6] although also other hypotheses exist [1, 6]. Recently, the causation of implantation-related performance degradation by dislocation loops, likely decorated with metallic impurities, could be substantiated [7, 8].

The agglomeration of implantation-induced self-interstitials (Is) via the formation of small interstitial clusters (SMICs) and their transformation to $\{311\}$ defects and even small loops has been addressed by a variety of models, e.g. [9, 10, 11, 12, 13, 14, 15], and is well described by them. This does not hold true for the high thermal budgets of solar cell fabrication. As we will show later (Sec. II), even the latest of them, the model of Zographos *et al.* [15] implemented in Sentaurus Process [16], fails then to reproduce two important qualitative aspects

(i) The predicted dissolution velocity at high temperatures is by orders of magnitude too high.
(ii) The simulated growth of the mean loop radius does not saturate for long annealing times at high temperatures, as would be expected from theory and experiment.

Point (i) implies that for almost all relevant annealing conditions, the model of Zographos *et al.* [15] predicts a complete dissolution of loops. Thus, it cannot be used to establish correlations between processing conditions and cell performance. Point (ii) is more subtle and of lower priority: A quantitatively wrong prediction of the mean loop radius translates directly into a likewise wrong prediction of the proportionally related dislocation-line density, which directly correlates to the recombination activity of loops [17, 18]. Two other loop models [13, 19] implemented in Sentaurus Process [20] suffer from even more severe problems for annealing processes with high thermal budgets. For an in-depth discussion of the modeling of dislocation loops the interested reader is referred to the review article of Claverie et al. [21] and the dissertation of one of the authors (F.A.W) [22].

In this paper, we extend the model of Zographos *et al.* [15] to overcome problem (i) (Sec. III). We succeed in doing so by accounting for the parallel ripening of faulted and perfect dislocation loops. The new model is able to provide meaningful information about the local densities and sizes of insufficiently annealed dislocation loops [7, 8]. Subsequently, we analyze the late stages of Ostwald ripening, which leads us to sketch a model that is able to resolve problem (ii) (Sec. IV). Finally, we conclude the paper (Sec. V). We start with a brief discussion of the model of Zographos *et al.*.

II. The model of Zographos *et al.*

Zographos *et al.* [15] model the mean concentration of loops D_L and the concentration of self-interstitials (Is) C_L comprised in these loops by

$$\partial_t C_\mathrm{L} = R_\mathrm{L}^{311} + R_\mathrm{L}^\mathrm{I}, \tag{1a}$$

$$\partial_t D_\mathrm{L} = \widetilde{R}_\mathrm{L}^{311} + \widetilde{R}_\mathrm{L}^\mathrm{I}. \tag{1b}$$

These distributions depend on time and position. The reaction terms that describe the unfaulting reaction from $\{311\}$ defects to loops are given by

$$R_\mathrm{L}^{311} = k_\mathrm{L}^{311} C_{311} C_{311}, \tag{2a}$$

$$\widetilde{R}_\mathrm{L}^{311} = k_\mathrm{L}^{311} \widetilde{k}_\mathrm{L}^{311} C_{311} D_{311}, \tag{2b}$$

where D_{311} and C_{311} denote the concentration of $\{311\}$ defects and the concentration of Is bound in $\{311\}$ defects, in complete analogy to the meaning of D_L and C_L. k_L^{311} is described by an Arrhenius law [20]. Zographos *et al.* [15] set $\widetilde{k}_\mathrm{L}^{311} = \frac{1}{2}$, which means that $\{311\}$ defects with twice the mean size unfault to loops.

The interaction of loops with free Is is described by

$$R_\mathrm{L}^\mathrm{I} = k_\mathrm{L}^\mathrm{I} 2\pi^2 \overline{r_\mathrm{L}} D_\mathrm{I} (C_\mathrm{I} - C_\mathrm{I,L}^*) D_\mathrm{L}, \tag{3a}$$

$$\widetilde{R}_\mathrm{L}^\mathrm{I} = -k_\mathrm{L}^\mathrm{I} 2\pi^2 \overline{r_\mathrm{L}} D_\mathrm{I} C_\mathrm{I,L}^* \frac{D_\mathrm{L} D_\mathrm{L}}{C_\mathrm{L}} = -\frac{k_\mathrm{L}^\mathrm{I} 2\pi D_\mathrm{I}}{\overline{r_\mathrm{L}} n_\mathrm{L}} C_\mathrm{I,L}^* D_\mathrm{L}, \tag{3b}$$

F. A. Wolf and A. Martinez-Limia are with Corporate Research, Robert Bosch GmbH, Robert-Bosch-Platz 1, 70839 Gerlingen-Schillerhöhe, Germany.

D. Stichtenoth is with Bosch Solar Energy, Arnstadt, Germany.

P. Pichler is with the Fraunhofer Institute for Integrated Systems and Device Technology, Schottkystrasse 10, 91058 Erlangen, Germany and with the Chair of Electron Devices, University of Erlangen-Nuremberg, Cauerstrasse 6, 91058 Erlangen, Germany.

Manuscript received April 19, 2005; revised December 27, 2012.

where C_I is the concentration of free Is, k_L^I is a calibration constant and D_I the diffusion coefficient of Is. The mean loop radius $\overline{r_\mathrm{L}}$ and the equilibrium concentration of Is in the vicinity of a loop $C_\mathrm{I,L}^*$ are defined by

$$\overline{r_\mathrm{L}} = \sqrt{\frac{C_\mathrm{L}}{D_\mathrm{L} n_\mathrm{L} \pi}} \qquad \text{and} \qquad C_\mathrm{I,L}^* = C_\mathrm{I}^* e^{\Delta E_\mathrm{L}(\overline{r_\mathrm{L}})/kT}, \quad (4)$$

where n_L is the atomic areal density in the close-packed $\{311\}$ planes. For the formation energy per I in faulted dislocation loops $\Delta E_\mathrm{L}(\overline{r_\mathrm{L}})$, Zographos *et al.* [15] used the definition

$$\Delta E_\mathrm{L}(\overline{r_\mathrm{L}}) = \frac{\gamma\Omega}{b} + \frac{Gb\Omega}{4\pi\overline{r_\mathrm{L}}(1-\nu)} \ln(8\overline{r_\mathrm{L}}/b). \quad (5)$$

Therein, γ is the stacking-fault energy per unit volume, Ω the atomic volume, b the modulus of the Burger's vector of the loop, G the shear modulus of Si and ν its Poisson ratio. With these equations, the loop model is completely defined.

In the present paper, the focus is on the phase of the annealing process in which the last step of the I cluster nucleation process, the unfaulting reaction from $\{311\}$ defects to loops, is completed. At this point, almost all $\{311\}$ defects have vanished, so that $R_\mathrm{L}^{311} \simeq 0$ and $\widetilde{R}_\mathrm{L}^{311} \simeq 0$, and one is left to discuss, instead of Eqs. (1), the equations $\partial_t C_\mathrm{L} = R_\mathrm{L}^\mathrm{I}$ and $\partial_t D_\mathrm{L} = \widetilde{R}_\mathrm{L}^\mathrm{I}$.

A. Dissolution velocity of dislocation loops

The first fundamental problem that arises from the model of Zographos *et al.* [15] is a qualitative overestimation of the dissolution velocity of loops. This is illustrated in Fig. 1 for the areal density of loops $\mathcal{N}_\mathrm{L} = \int_0^{t_\mathrm{W}} dx\, D_\mathrm{L}(x)$, where we integrated over the wafer thickness t_W. We empirically checked that this problem cannot be resolved by recalibrating the value [16] of the sole free parameter k_L^I in Eqs. (3). Fig. 1(a) shows that the model yields satisfying results for temperatures up to 950 °C. But at 1000 °C and 1050 °C, the simulated dissolution is much too rapid. In the case of Fig. 1(b), where many more implantation-induced Is have been produced, the dissolution velocity is qualitatively wrong even at 950 °C.

B. Late stages of Ostwald ripening

The other fundamental problem of the model of Zographos *et al.* [15] concerns the time evolution of the mean loop radius $\overline{r_\mathrm{L}}$. From Eq. (4), the time evolution of $\overline{r_\mathrm{L}}$ is obtained using Eqs. (1) and Eqs. (3) as

$$\frac{d\overline{r_\mathrm{L}}}{dt} = \frac{k_\mathrm{L}^\mathrm{I} \pi D_\mathrm{I}}{n_\mathrm{L}} C_\mathrm{I}. \quad (6)$$

Now consider the case $C_\mathrm{I} \simeq C_\mathrm{I}^*$, i.e. the time during annealing at which the number of loops has considerably decreased. The remaining ones are so large that they can gain relatively few energy by exchanging Is. In this situation, Eq. (6) predicts a linearly diverging time evolution of $\overline{r_\mathrm{L}}$ while, in reality, the loop radius growth is much weaker [25, 23]. As soon as the surface and other sinks for Is become dominant, loops finally start shrinking again, although slowly, as Ostwald ripening ensures that rather the number of loops decreases, than their size. The described phenomenon is illustrated in Fig. 2. For all the experiments shown, temperatures are sufficiently high and annealing times sufficiently long so that Ostwald ripening is in its final stage. In all panels of Fig. 2, the experiments shown indicate a saturation of the loop radius with time. By contrast, the solid lines calculated using the model of Zographos *et al.* [15] display a diverging radius evolution.

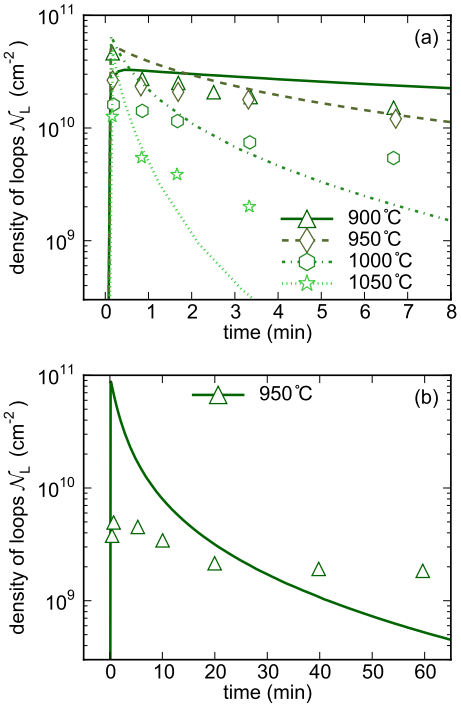

Fig. 1. Time evolution of the areal loop density $\mathcal{N}_\mathrm{L}$ during annealing. (a) Rapid thermal annealing (RTA) after a Ge implant of $2{\cdot}10^{15}$ cm^{-2} at 150 keV, experimental data from [23]. (b) RTA after a B implant of $1{\cdot}10^{15}$ cm^{-2} at 30 keV, experimental data from [24]. Symbols depict experimental results, lines simulation results. Simulations were done with the model of Zographos *et al.* [15] in the implementation of [16].

III. Parallel Ripening of Faulted and Perfect Loops

The model of Zographos *et al.* [15] describes faulted loops (FLs) and makes correct predictions for experiments with low thermal budgets, while failing for high temperatures and extended annealing times. This failure can be explained with the following experimental observation. For low thermal budgets, mainly FLs are observed [27, 28, 29, 30]. For high thermal budgets, during which loops undergo strong Ostwald ripening and grow considerably, almost only perfect loops (PLs) are observed [31, 32, 28, 33, 34, 29]. This behavior is due to the well-known fact that for large loop sizes, perfect loops are more stable than faulted loops. Our model extends Zographos' model to describe not only FLs, but to also include PLs. While modeling FLs is still necessary to correctly describe the early stages of a high-thermal-budget process, modeling the different reaction dynamics of PLs allows to describe the late stages. Hence, our new model needs to physically describe both types of loops.

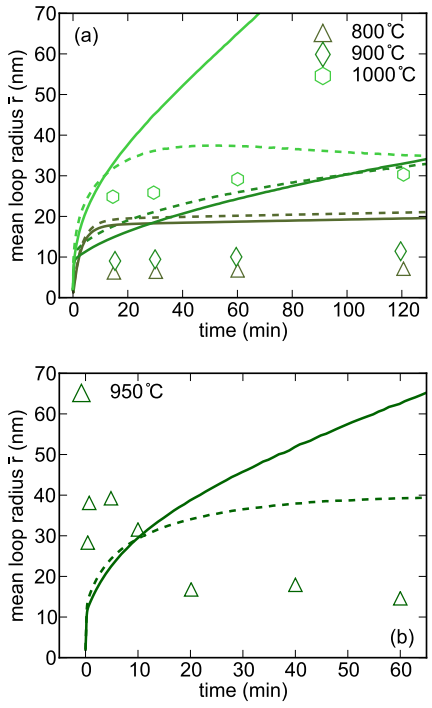

Fig. 2. Time evolution of the mean loop radius $\overline{r_{\rm L}}$ during annealing. (a) RTA after an Si implant of $1{\cdot}10^{15}$ cm^{-2} at 50 keV, experimental data from [26]. (b) RTA after a B implant of $1{\cdot}10^{15}$ cm^{-2} at 30 keV, experimental data from [24]. Symbols depict experimental results, lines simulation results. Solid lines were calculated with the model of Zographos *et al.* [15] in the implementation of [16]. Dashed lines were calculated with the same parameters using the model presented in Sec. IV.

For intermediate thermal budgets, a transition from the state with more faulted loops to the state with more perfect loops takes place. This transition has traditionally been assumed to result from an unfaulting reaction [35], meaning that a faulted loop, in our cases always a Frank partial dislocation, reacts with a Shockley partial dislocation to produce a perfect dislocation loop. In contradiction to that, several authors have observed independent time evolutions of the FL and the PL ensembles, clearly identifying two different Ostwald ripening mechanisms [28, 27, 29]. This observation suggests that a second explanation for the FL-PL transistion is more likely: Rather than by a direct unfaulting reaction, the transition occurs as the two ensembles of different loop types exchange Is among each other. Our model is based on this second explanation.

A. Energy of faulted and perfect dislocation loops

The energy associated with a dislocation loop consists of the elastic energy of the surrounding strain fields, its core energy and a potential stacking-fault energy. The faulted loops most frequently observed in Si are Frank partial loops, which lie in $\{111\}$ planes and have a Burger's vector $\boldsymbol{b}_{\rm FL} = \frac{a}{3}[111]$ with $a = 5.43$ Å denoting the size of the silicon unit cell. Perfect loops in fcc lattices also lie in $\{111\}$ planes but have a Burger's vector of $\boldsymbol{b}_{\rm PL} = \frac{a}{2}[110]$. Their respective elastic energies are [35, 27]

$$E^{\rm el}_{\rm FL} = \frac{r_{\rm L} G b^2_{\rm FL}}{2(1-\nu)} \ln(r_1/r_0),\ b^2_{\rm FL} = \frac{a^2}{3}, \tag{7a}$$

$$E^{\rm el}_{\rm PL} = \frac{r_{\rm L} G b^2_{\rm PL}}{2(1-\nu)} \left(1-\frac{\nu}{6}\right) \ln(r_1/r_0),\ b^2_{\rm PL} = \frac{a^2}{2}. \tag{7b}$$

Linear elasticity theory is only valid at some distance away from the core. This distance is characterized by r_0 for which we assume $r_0 = b_{\rm FL}/4$ [27]. For r_1, roughly characterizing the extent of the lattice distortions, we assume $r_1 = 2r_{\rm L}$ [36, 35].

The energy $E^{\rm core}$ stored in the core can only be accessed by atomistic calculations, albeit with a low precision. The stacking-fault energy of faulted loops is $\gamma \simeq 70\,{\rm mJ/m^2}$ per atomic volume. Adding these terms to Eqs. (7a) and (7b), one obtains

$$E_{\rm FL} = \gamma\pi r_{\rm L}^2 + \frac{r_{\rm L} G b^2_{\rm FL}}{2(1-\nu)} (\ln(8r_{\rm L}/b_{\rm FL}) - 1 + A_{\rm FL}), \tag{8a}$$

$$E_{\rm PL} = \frac{r_{\rm L} G b^2_{\rm PL}}{2(1-\nu)} \left(1-\frac{\nu}{6}\right) (\ln(8r_{\rm L}/b_{\rm FL}) - 1 + A_{\rm PL}). \tag{8b}$$

The constants $A_{\rm FL,PL}$ have been introduced to represent the core energy via $E^{\rm core}_{\rm FL} = A_{\rm FL} \frac{r_{\rm L} G b^2_{\rm FL}}{2(1-\nu)}$ and $E^{\rm core}_{\rm PL} = A_{\rm PL} \frac{r_{\rm L} G b^2_{\rm PL}}{2(1-\nu)} \left(1-\frac{\nu}{6}\right)$, respectively. Their values will be discussed in more detail below. The constant -1 was introduced in the last expressions in brackets to account for a frequent convention in the literature, ensuring a stress-free boundary at the upper integration limit for the elastic energy r_1 [37, 38].

Although the functional form of the expressions (8) is undebated, the numerical values for the integration boundaries r_1, r_0 and the core energy $E^{\rm core}$ are only roughly known [39]. If, in addition, the loop is not ciruclar but shaped like an n-sided regular polygon, which can be a reasonable assumption for PLs, a further constant has to be added to $A_{\rm FL,PL}$ [40]. One should therefore be satisfied with specifying a numerical range of meaningful values for these parameters. Surveying the literature, one finds the following values (We abbreviate $A_{\rm FL,PL}$ with $A_{\rm L}$.): Some authors choose $A_{\rm L} = 0$ [15, 23, 19, 38, 41] and others $A_{\rm L} = 1$ [27, 35] and all of these either choose $r_0 = b/4$ or $r_0 = b$. Again others employ a very different expression $A_{\rm L} = \frac{2\nu-1}{4\nu-4}$ [42, 13]. Having made the choice for $r_0 = b/4$ and $r_1 = 2r_{\rm L}$ in Eqs. (8), all uncertainty is accommodated in $A_{\rm L}$. Assuming that the true value of r_0 is in the range $r_0 \in [b/4, 4b]$ [43, 35, 44] and that the true core-energy-related component of $A_{\rm L}$ is in the range $[0, 1]$, one obtains the following range of meaningful values for $A_{\rm L} \in [-2.77, 1]$.

B. Energy per self-interstitial in a dislocation loop

The energy necessary to incorporate one I in a loop is $\Delta E_{\rm L} = \frac{dE}{dN} = \frac{1}{n_{\rm L} 2\pi r_{\rm L}} \frac{dE}{dr_{\rm L}}$. Using Eq. (8), we obtain

$$\Delta E_{\rm FL} = \gamma\Omega/b_{\rm FL} + \frac{G b_{\rm FL}\Omega}{4\pi r_{\rm L}(1-\nu)} (\ln(8r_{\rm L}/b_{\rm FL}) + A_{\rm FL}), \tag{9a}$$

$$\Delta E_{\rm PL} = \left(\frac{6-\nu}{4}\right) \frac{G b_{\rm FL}\Omega}{4\pi r_{\rm L}(1-\nu)} (\ln(8r_{\rm L}/b_{\rm FL}) + A_{\rm PL}). \tag{9b}$$

The result of Eqs. (9) is shown in Fig. 3(a) for $A_{\rm FL} = 0$ and $A_{\rm PL} = 0$. The stability inversion occurs for loop sizes around

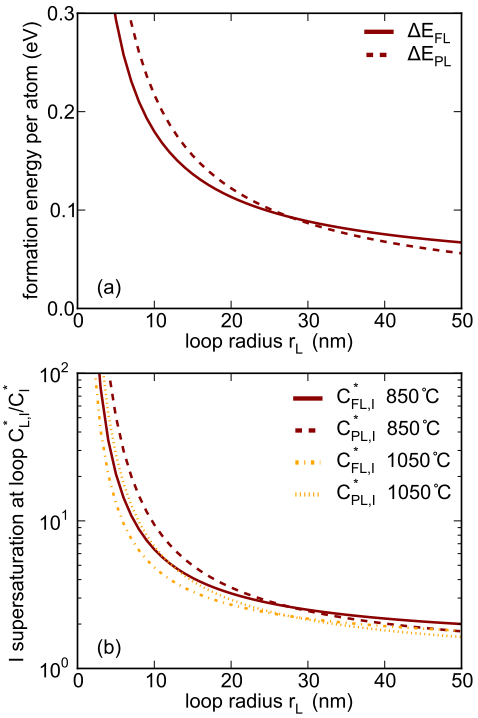

Fig. 3. Comparison of FL and PL formation energy (a) and I supersaturation in the vicinity of a loop (b). Parameters are given in the text.

30 nm, which is similar to the results of [27] and [29]. The parameters used for this calculation are given by $\gamma = 70\,\mathrm{mJ/m^2}$, $\Omega = 2\times10^{-23}\,\mathrm{cm^3}$, $G = 63.28\times10^5\,\mathrm{N/cm^2}$, $\nu = 0.28$, and $b_{\mathrm{FL}} = 0.3135\,\mathrm{nm}$. With that, $E_{\mathrm{sf}} = \gamma\Omega/b_{\mathrm{FL}} = 0.0279\,\mathrm{eV}$ and $\frac{Gb_{\mathrm{FL}}\Omega}{4\pi(1-\nu)} = 0.274\,\mathrm{eV\,nm}$. The even more interesting quantity is given by $C^*_{\mathrm{L,I}} = C^*_{\mathrm{I}} e^{\Delta E(\overline{r_{\mathrm{L}}})/kT}$, see Eq. (4) and Fig. 3(b). Here, the stability inversion of Fig. 3 is amplified to an exponential behavior. $C^*_{\mathrm{L,I}}$ is responsible for the dissolution of loops due to interactions with external sinks or the other loop ensemble.

C. Summary of model equations

The equations for the parallel evolution of ensembles of FLs and PLs read, in complete consistence with the model presentation for only faulted loops in Sec. II,

$$\partial_t C_{\mathrm{FL}} = R^{311}_{\mathrm{FL}} + R^{\mathrm{I}}_{\mathrm{FL}}, \tag{10a}$$
$$\partial_t D_{\mathrm{FL}} = \widetilde{R}^{311}_{\mathrm{FL}} + \widetilde{R}^{\mathrm{I}}_{\mathrm{FL}}, \tag{10b}$$
$$\partial_t C_{\mathrm{PL}} = R^{311}_{\mathrm{PL}} + R^{\mathrm{I}}_{\mathrm{PL}}, \tag{10c}$$
$$\partial_t D_{\mathrm{PL}} = \widetilde{R}^{311}_{\mathrm{PL}} + \widetilde{R}^{\mathrm{I}}_{\mathrm{PL}}. \tag{10d}$$

where the functional forms of the terms R^{311}_{FL}, $\widetilde{R}^{311}_{\mathrm{FL}}$, R^{311}_{PL} and $\widetilde{R}^{311}_{\mathrm{PL}}$ have been defined in Eqs. (2) for a general loop. All of these terms contain either the reaction rate k^{311}_{FL} or k^{311}_{PL}, which determine the unfaulting rate of $\{311\}$ defects to loops. In agreement with the experimental observation that PLs are only observed for higher temperatures, we choose k^{311}_{FL} to have a lower activation energy than k^{311}_{PL}. The terms $\widetilde{R}^{311}_{\mathrm{FL}}$ and $\widetilde{R}^{311}_{\mathrm{PL}}$ contain furthermore the factors $\widetilde{k^{311}_{\mathrm{FL}}}$ and $\widetilde{k^{311}_{\mathrm{PL}}}$, respectively. In agreement with the experimental observation of Stowe [29], that perfect loops nucleate at a larger mean radius than faulted loops, we choose $\widetilde{k^{311}_{\mathrm{PL}}} = 0.05$ in comparison to $\widetilde{k^{311}_{\mathrm{FL}}} = 0.5$ [15] for faulted loops. Finally, it should be kept in mind that the expressions of the formation energies per I Eqs. (9) to be used for $C^*_{\mathrm{I,L}}$ are different for faulted and perfect loops.

As the result of a calibration based on a variety of experiments, we set $k^{311}_{\mathrm{FL}} = 9\cdot10^{-5}\cdot e^{-4.2\,\mathrm{eV}/kT}\,\mathrm{cm^3/s}$ for faulted loops while keeping $\widetilde{k^{311}_{\mathrm{FL}}}$, $k^{\mathrm{I}}_{\mathrm{FL}}$ and $A_{\mathrm{FL}} = 0$ as in Sentaurus Process [16]. For perfect loops, we set $k^{311}_{\mathrm{PL}} = 4\cdot10^5\cdot e^{-6\,\mathrm{eV}/kT}\,\mathrm{cm^3/s}$, $\widetilde{k^{311}_{\mathrm{PL}}} = 0.05$, $k^{\mathrm{I}}_{\mathrm{PL}} = 1.5\cdot10^{-7}\cdot e^{1.5\,\mathrm{eV}/kT}$, and $A_{\mathrm{PL}} = -2.65$.

D. Comparison with the experiment

We note that for low temperatures or short annealing times, the model extension presented gives virtually the same results as the original model of Zographos *et al.* [15]. Thus, we only discuss high temperatures and extended times. The implantation conditions for these experiments were modeled with the native Monte Carlo implantation simulator of Sentaurus Process, using the default parameters [20]. Sentaurus Process then accounts for amorphization and solid-phase epitaxial regrowth by setting the concentration of implantation-induced Is and Vs in amorphized regions to zero. Only Is that remain behind the amorph-crystalline boundary can therefore contribute to the formation of dislocation loops. In Fig. 4, simulations for 1000 °C are compared to experiments. At this temperature, perfect loops become relevant for the implantation conditions of [28] and they dominate the total density of loops for times exceeding about 4 min. Due to the stability inversion, PLs dissolve slowlier and have a larger mean radius than FLs. Fig. 5 provides a further example for different implantation conditions. Fig. 6 compares our model with experiments for a wide range of temperatures, showing good agreement in contrast to the results obtained with the model of Zographos *et al.* shown in Fig. 1.

While the preceding experimental conditions comprised the well-studied conditions of amorphizing Si and Ge implants, for solar cells, we are also interested in non-amorphizing B implants. For the example of a B implant of $1\cdot10^{15}\,\mathrm{cm^{-2}}$ at 30 keV annealed for 15 min at 900 °C, Fig. 7 shows simulations of the as-implanted and annealed boron concentrations. It also compares simulated and experimentally measured values for the depth dependence of the dislocation-line density $\rho_{\mathrm{L}} = 2\pi\overline{r_{\mathrm{L}}}D_{\mathrm{L}}$. While the experimental values correspond to a mean value for FLs and PLs, the dislocation-line densities for both types are resolved in the simulations.

Fig. 8(a) and (b) show the time evolution of loop densities during RTA and furnace anneals after B implantation. Our model reasonably compares with experiment, in contrast to the model of Zographos *et al.* [15], see Fig. 1.

IV. Modeling the Saturation of Ostwald Ripening

While the model of the preceding section for the first time enables the simulation of dislocation loops in the parameter regime of solar cell processes, this section is devoted to a more subtle and weaker effect that arises for these processes. In

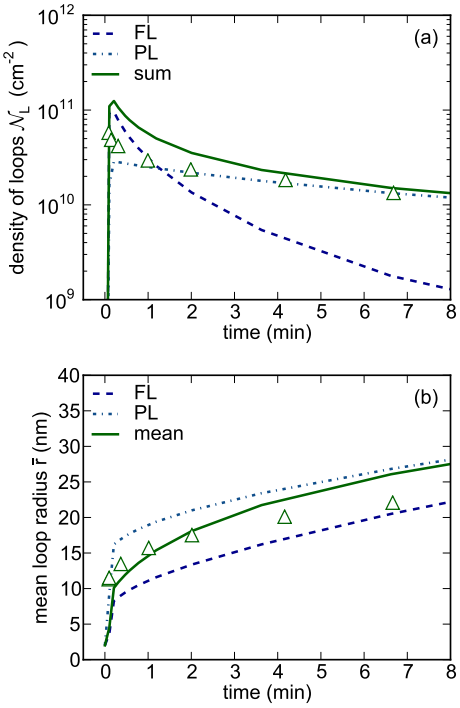

Fig. 4. Loop evolution during RTA annealing at 1000 °C following a Si implant of $1{\cdot}10^{16}$ cm^{-2} at 50 keV. Experimental data from [28].

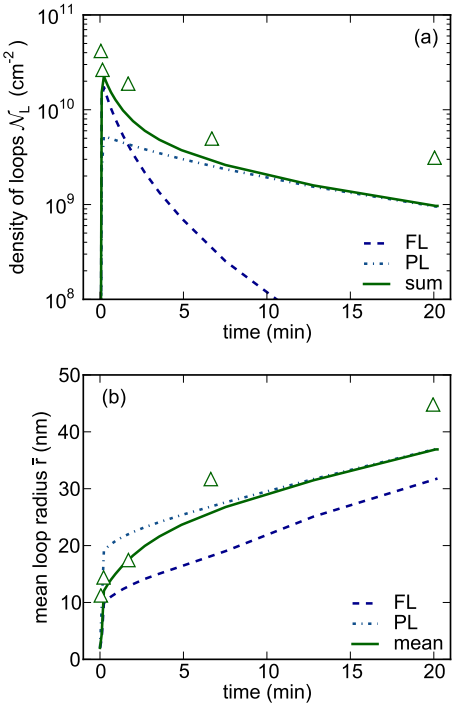

Fig. 5. Loop evolution during RTA annealing at 1000 °C following a Ge implant of $2{\cdot}10^{15}$ cm^{-2} at 150 keV. Experimental data from [45].

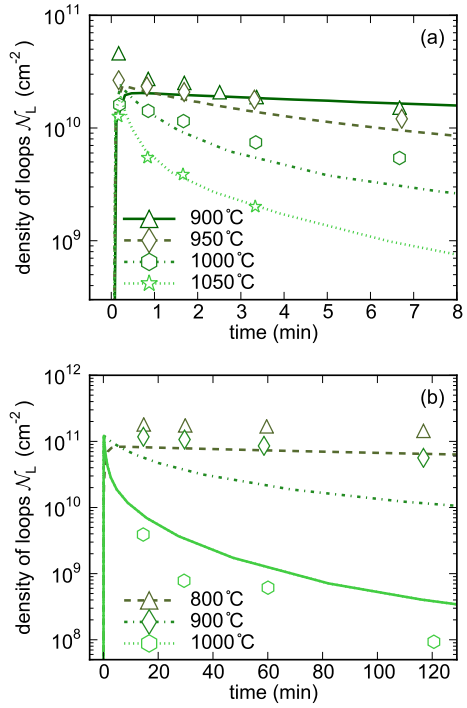

Fig. 6. Time evolution of the areal loop density $\mathcal{N}_L$ (sum of FL and PL densities) during annealing. (a) Rapid thermal annealing (RTA) after an Ge implant of $2{\cdot}10^{15}$ cm^{-2} at 150 keV, experimental data from [23]. Compare this to Fig. 1. (b) RTA after an Si implant of $1{\cdot}10^{15}$ cm^{-2} at 50 keV, experimental data from [26].

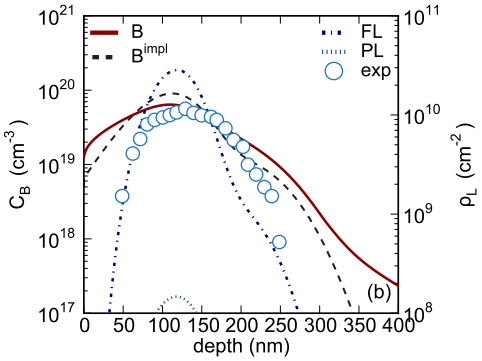

Fig. 7. The as-implanted and annealed B profile are shown on the left y-axis. The dislocation-line densities for perfect (PL) and faulted loops (FL) are shown on the right y-axis, together with experimental data for the mean dislocation-line density. For this experiment a B dose of $1{\cdot}10^{15}$ cm^{-2} was implanted at 30 keV and annealed at 900 °C for 15 min. With this low thermal budget, FLs can be seen to be still strongly dominant in the simulation. Only for higher thermal budgets, as shown in Fig. 8(a), PLs start to dominate. Experimental data from [29, p. 130].

Fig. 2 and the respective discussion, we showed that the model of Zographos *et al.* predicts a linearly diverging loop radius while experiments indicate a much weaker increase if not reduction. As the mean loop radius enters the disloction line density, which directly relates to the recombination activity of loops, this model artifact should reduce the quantitative predicitive power of the model of Zographos *et al.*. We sketch an idea that overcomes this artifact at the expense of an only slightly more complicated model definition.

During annealing, Is will be exchanged among the extended defects as well as between them and the surface or other sources and sinks. The former processes is conservative and leads always to an increase of the mean loop radius $\overline{r_L}$ of the ensemble. The latter process is non-conservative and

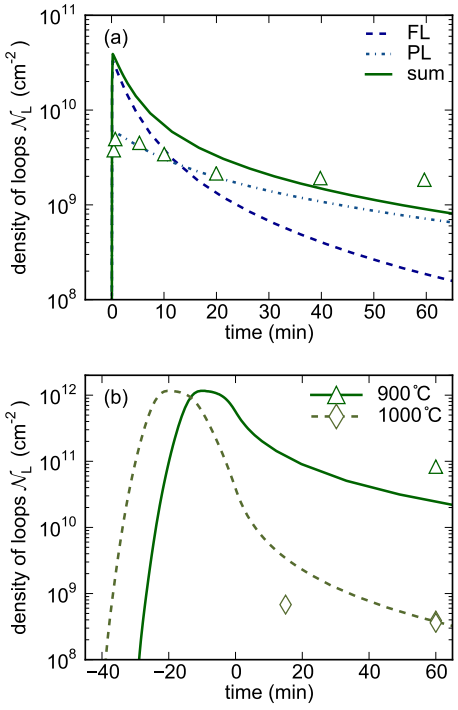

Fig. 8. Time evolution of the areal loop density $\mathcal{N}_\mathrm{L}$ during annealing. (a) RTA at 950 °C after a B implant of $1{\cdot}10^{15}$ cm^{-2} at 30 keV, experimental data from [24]. Compare this to Fig. 1. (b) Loop evolution during furnace annealing, ramp-up at 10 K/min starting at 600 °C. B implant of $1{\cdot}10^{16}$ cm^{-2} at 30 keV. Experimental data from [29]. Negative times refer to ramp-up and preannealing phases. Symbols depict experimental results, lines simulation results. If not specified otherwise, data points refer to the sum of FL and PL densities.

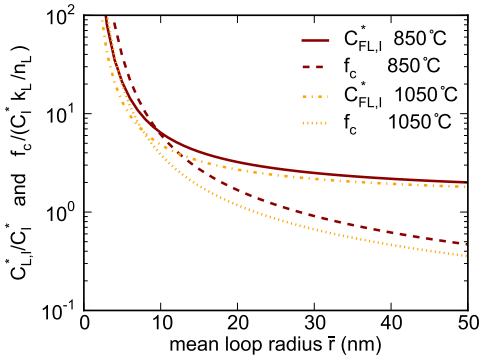

Fig. 9. Comparison of the quantities $C^*_{\mathrm{I,L}}$ and $f_c \propto (C^*_{\mathrm{I,L}}(\overline{r_\mathrm{L}} - \sigma_\mathrm{L}) - C^*_{\mathrm{I,L}}(\overline{r_\mathrm{L}} + \sigma_\mathrm{L}))$, see Eq. (13), which govern the non-conservative and the conservative processes during the evolution of the loop ensemble, respectively. Here, $\frac{\sigma_\mathrm{L}}{\overline{r_\mathrm{L}}} = 0.4$.

increases or decreases $\overline{r_\mathrm{L}}$. Although the distinction of these two processes has been acknowledged for a long time [25], it has never explicitly been taken into account by process simulation models. By explicitly accounting for these processes, we obtain a new loop model that gives rise to different loop-loop and loop-I reaction dynamics than the model of Zographos *et al.*.

A. Model equation ansatz

We make the following ansatz for the time evolution of the mean loop radius $\overline{r_\mathrm{L}}$

$$\frac{d\overline{r_\mathrm{L}}}{dt} = f_{nc}(\overline{r_\mathrm{L}}) + f_c(\overline{r_\mathrm{L}}), \tag{11}$$

where f_{nc} and f_c are functions of $\overline{r_\mathrm{L}}$ that correspond to the non-conservative and conservative contributions to loop growth. The natural choice for f_{nc} is known to be [19]

$$f_{nc}(\overline{r_\mathrm{L}}) = \frac{k_\mathrm{L}}{n_\mathrm{L}}(C_\mathrm{I} - C^*_{\mathrm{I,L}}(\overline{r_\mathrm{L}})), \tag{12}$$

where k_L is a reaction rate. In the conservative regime, when no other comparable sinks or sources but the loop ensemble itself are present, f_{nc} should be zero. This holds indeed true as then $C_\mathrm{I} \simeq C^*_{\mathrm{I,L}}(\overline{r_\mathrm{L}})$.

For the conservative contribution to loop growth $f_c(\overline{r_\mathrm{L}})$, we make the ansatz

$$f_c(\overline{r_\mathrm{L}}) = \frac{k_\mathrm{L}}{n_\mathrm{L}}(C^*_{\mathrm{I,L}}(\overline{r_\mathrm{L}} - \sigma_\mathrm{L}) - C^*_{\mathrm{I,L}}(\overline{r_\mathrm{L}} + \sigma_\mathrm{L})) \tag{13}$$

where σ_L has the meaning of the variance of the loop-size distribution. The choice is motivated as follows. Ostwald ripening is due to the conservative exchange of Is from small loops to large loops. In analogy to the ansatz of Burton and Speights [25], who described the evolution of a loop with radius r_L as a result of the interaction with the mean I concentration $C^*_{\mathrm{I,L}}(\overline{r_\mathrm{L}})$, Eq. (13) describes the radius evolution of a loop with radius $\overline{r_\mathrm{L}} + \sigma_\mathrm{L}$ as a result of the interaction with the emitted I concentration of a smaller loop with radius $\overline{r_\mathrm{L}} - \sigma_\mathrm{L}$. As the simulation cannot account for all processes that occur between loops of the full loop-size distribution, we assume that the exchange of Is between loops of size $\overline{r_\mathrm{L}} - \sigma_\mathrm{L}$ and $\overline{r_\mathrm{L}} + \sigma_\mathrm{L}$ should be a representative approximation for these processes. Note that also for the choice of f_{nc}, we neglected the details of the loop-size distribution.

In the early stages of the annealing process, when many small loops are present, the conservative exchange of Is (13) will govern the loop evolution, while, at a stage at which loops have become large, the non-conservative contributions (12) may become more important. Our choice for f_c reflects this transition: f_c takes high values for low values of $\overline{r_\mathrm{L}}$ and tends to zero for high values of $\overline{r_\mathrm{L}}$, i.e. in the late-stage regime. This behavior is obvious in Fig. 9. Furthermore, f_c reflects the fact that a loop-size distribution with a large size variance σ_L displays faster Ostwald ripening than a distribution with a small variance.

We note that we always choose $\sigma_\mathrm{L} \propto \overline{r_\mathrm{L}}$. As the size distribution function of loops, normalized to the mean loop radius $\overline{r_\mathrm{L}}$, is time-independent for conservative Ostwald ripening [46, 25] as well as in the early stage when the conservative exchange of Is dominates, the normalized variance $\sigma_\mathrm{L}/\overline{r_\mathrm{L}}$ of the distribution must be time-independent, too. In the late-stage phase, $f_c \simeq 0$ holds and, by that, the value of σ_L becomes unimportant. An additional equation for the time evolution of σ_L, which corresponds to the third moment of the loop-size distribution, is therefore unnecessary. Consequently, the preceding definition of a two-moment model automatically corresponds to a three-moment model.

B. Summary of model equations and comparison to experiment

Before, we obtained the time evolution of $\overline{r_\mathrm{L}}$ in Eq. (6) from Eqs. (1) with R_L^I and $\widetilde{R}_\mathrm{L}^\mathrm{I}$ defined in Eqs. (3). Now we use the expression for $\overline{r_\mathrm{L}}$ in Eq. (11) and the expression of R_L^I of Eqs. (3) to obtain an expression for $\widetilde{R}_\mathrm{L}^\mathrm{I}$. Adopting the notation of [15], we set the constant $k_\mathrm{L} = \pi k_\mathrm{L}^\mathrm{I} D_\mathrm{I}$ and obtain

$$R_\mathrm{L}^\mathrm{I} = k_\mathrm{L}^\mathrm{I} 2\pi^2 \overline{r_\mathrm{L}} D_\mathrm{I} (C_\mathrm{I} - C_\mathrm{I,L}^*(\overline{r_\mathrm{L}})) D_\mathrm{L}, \tag{14a}$$

$$\widetilde{R}_\mathrm{L}^\mathrm{I} = -\frac{k_\mathrm{L}^\mathrm{I} 2\pi D_\mathrm{I}}{\overline{r_\mathrm{L}} n_\mathrm{L}} (C_\mathrm{I,L}^*(\overline{r_\mathrm{L}} - \sigma_\mathrm{L}) - C_\mathrm{I,L}^*(\overline{r_\mathrm{L}} + \sigma_\mathrm{L})) D_\mathrm{L}. \tag{14b}$$

This is to be compared with the model equations of [15] given in Eqs. (3). The difference between the model we propose and the one of [15] is that instead of the term $(C_\mathrm{I,L}^*(\overline{r_\mathrm{L}} - \sigma_\mathrm{L}) - C_\mathrm{I,L}^*(\overline{r_\mathrm{L}} + \sigma_\mathrm{L}))$ in the equation for $\widetilde{R}_\mathrm{L}^\mathrm{I}$, [15] employ $C_\mathrm{I,L}^*(\overline{r_\mathrm{L}})$. We have already compared these terms in Fig. 9.

We compare the results of our model (14) with the results of Zographos' model in Fig. 2. Our model clearly allows to identify the early and late stages of Ostwald ripening via the observation of two time-scales in the reaction dynamics: In the early stage, when the conservative exchange of Is dominates, the loop radius increases strongly $\propto \sqrt{t}$ [25], while for long times where the non-conservative exchange dominates, it increases only weakly or even saturates. Zographos' model, by contrast, leads to a strong loop-radius growth also for long times when considering high temperatures.

For the calculation of Fig. 2 we used $\sigma_\mathrm{FL}/\overline{r_\mathrm{FL}} = 0.4$ with all other parameters as in the preceding section. Only for k_FL^{311} the original value of [16] was used.

V. Conclusion

We presented a dislocation-loop model for the concurrent growth of faulted and perfect dislocation loops and sketched a model that reproduces the saturation of Ostwald ripening. In comparison to established work, both approaches improve the agreement with experiments particularly for high thermal budgets. The model has already proven its viability for solar-cell processing conditions [7, 8].

References

[1] B. J. Pawlak, T. Janssens, S. Singh, I. Kuzma-Filipek, J. Robbelein, N. E. Posthuma, J. Poortmans, F. Cristiano, and E. M. Bazizi, "Studies of implanted boron emitters for solar cell applications," *Progress in Photovoltaics: Research and Applications*, vol. 20, no. 1, pp. 106–110, 2012. URL: http://dx.doi.org/10.1002/pip.1106

[2] M. G. Kang, J.-H. Lee, H. Boo, S. J. Tark, H. C. Hwang, W. J. Hwang, H. O. Kang, and D. Kim, "Effects of annealing on ion-implanted Si for interdigitated back contact solar cell," *Current Applied Physics*, vol. 12, no. 6, pp. 1615–1618, 2012. URL: http://dx.doi.org/10.1016/j.cap.2012.05.035

[3] J. Benick, R. Müller, N. Bateman, M. Hermle, and S. Glunz, "Fully implanted *n*-type PERT solar cells," *EU PVSEC Proceedings*, vol. 27, pp. 676–679, 2012. URL: http://dx.doi.org/10.4229/27thEUPVSEC2012-2BO.7.5

[4] W. Ho, Y.-H. Huang, W.-W. Hsu, Y.-Y. Chen, and C. Liu, "Ion implanted boron emitter *n*-silicon solar cells with wet oxide passivation," in *Photovoltaic Specialists Conference (PVSC), 2011 37th IEEE*, june 2011, pp. 001 058 –001 060. URL: http://dx.doi.org/10.1109/PVSC.2011.6186134

[5] A. Florakis, T. Janssens, E. Rosseel, B. Douhard, J. Delmotte, E. Cornagliotti, J. Poortmans, and W. Vandervorst, "Simulation of the anneal of ion implanted boron emitters and the impact on the saturation current density," *Energy Procedia*, vol. 27, no. 0, pp. 240–246, 2012. URL: http://dx.doi.org/10.1016/j.egypro.2012.07.058

[6] K. R. C. Mok, R. C. G. Naber, and L. K. Nanver, "Insights to emitter saturation current densities of boron implanted samples based on defects simulations," *AIP Conference Proceedings*, vol. 1496, no. 1, pp. 245–248, 2012. URL: http://dx.doi.org/10.1063/1.4766534

[7] J. Krügener, F. A. Wolf, R. Peibst, F. Kiefer, C. Schöllhorn, A. Grohe, R. Brendel, and H. J. Osten, "Correlation of dislocation line densities and emitter saturation current densities of ion implanted boron emitters," in *23rd Photovoltaic Science and Engineering Conference (PVSEC)*, 2013, pp. 1–0–31.

[8] J. Krügener, R. Peibst, F. A. Wolf, E. Bugiel, T. Ohrdes, F. Kiefer, C. Schöllhorn, A. Grohe, R. Brendel, and H. J. Osten, "Electrical and structural analysis of crystal defects after high-temperature rapid thermal annealing of highly boron ion-implanted emitters," *to be submitted to IEEE Journal of Photovoltaics*, 2014.

[9] A. H. Gencer and S. T. Dunham, "A predictive model for transient enhanced diffusion based on evolution of {311} defects," *Journal of Applied Physics*, vol. 81, no. 2, pp. 631–636, 1997. URL: http://dx.doi.org/10.1063/1.364204

[10] N. E. B. Cowern, G. Mannino, P. A. Stolk, F. Roozeboom, H. G. A. Huizing, J. G. M. van Berkum, F. Cristiano, A. Claverie, and M. Jaraíz, "Energetics of self-interstitial clusters in Si," *Phys. Rev. Lett.*, vol. 82, pp. 4460–4463, May 1999. URL: http://dx.doi.org/10.1103/PhysRevLett.82.4460

[11] M. Law and K. Jones, "A new model for {311} defects based on in situ measurements," in *Electron Devices Meeting (IEDM), Technical Digest. International*, 2000, pp. 511–514. URL: http://dx.doi.org/10.1109/IEDM.2000.904367

[12] D. Stiebel, P. Pichler, and N. E. B. Cowern, "A reduced approach for modeling the influence of nanoclusters and {113} defects on transient enhanced diffusion," *Applied Physics Letters*, vol. 79, no. 16, pp. 2654–2656, 2001. URL: http://dx.doi.org/10.1063/1.1406147

[13] I. Avci, M. E. Law, E. Kuryliw, A. F. Saavedra, and K. S. Jones, "Modeling extended defect ({311} and dislocation) nucleation and evolution in silicon," *Journal of Applied Physics*, vol. 95, no. 5, pp. 2452–2460, 2004. URL: http://dx.doi.org/10.1063/1.1645644

[14] C. Zechner, N. Zographos, D. Matveev, and A. Erlebach, "Accurate and efficient TCAD model for the formation and dissolution of small interstitial clusters and {311}

defects in silicon," *Materials Science and Engineering: B*, vol. 124-125, no. 0, pp. 401–403, 2005. URL: http://dx.doi.org/10.1016/j.mseb.2005.08.010

[15] N. Zographos, C. Zechner, and I. Avci, "Efficient TCAD model for the evolution of interstitial clusters, {311} defects, and dislocation loops in silicon," *MRS Proceedings*, vol. 994, p. 0994 F10 01, April 2007. URL: http://dx.doi.org/10.1557/PROC-0994-F10-01

[16] SPAC, *Advanced Calibration for Sentaurus Process User Guide, Version G-2012.06, Synopsys, Inc., Mountain View, CA*, 2012.

[17] C. Donolato, "Modeling the effect of dislocations on the minority carrier diffusion length of a semiconductor," *Journal of Applied Physics*, vol. 84, no. 5, pp. 2656–2664, 1998. URL: http://dx.doi.org/10.1063/1.368378

[18] V. Kveder, M. Kittler, and W. Schröter, "Recombination activity of contaminated dislocations in silicon: A model describing electron-beam-induced current contrast behavior," *Phys. Rev. B*, vol. 63, p. 115208, Mar 2001. URL: http://dx.doi.org/10.1103/PhysRevB.63.115208

[19] R. Y. S. Huang and R. W. Dutton, "Experimental investigation and modeling of the role of extended defects during thermal oxidation," *Journal of Applied Physics*, vol. 74, no. 9, pp. 5821–5827, 1993. URL: http://dx.doi.org/10.1063/1.355306

[20] SP, *Sentaurus Process User Guide, Version G-2012.06, Synopsys, Inc., Mountain View, CA*, 2012.

[21] A. Claverie, B. Colombeau, B. de Mauduit, C. Bonafos, X. Hebras, G. Ben Assayag, and F. Cristiano, "Extended defects in shallow implants," *Applied Physics A*, vol. 76, pp. 1025–1033, 2003. URL: http://dx.doi.org/10.1007/s00339-002-1944-0

[22] F. A. Wolf, "Modeling of annealing processes for ion-implanted single-crystalline silicon solar cells," Ph.D. dissertation, University of Erlangen-Nuremberg, 2014.

[23] C. Bonafos, D. Mathiot, and A. Claverie, "Ostwald ripening of end-of-range defects in silicon," *Journal of Applied Physics*, vol. 83, no. 6, pp. 3008–3017, 1998. URL: http://dx.doi.org/10.1063/1.367056

[24] M. Milosavljević, M. Lourenco, G. Shao, R. Gwilliam, and K. Homewood, "Optimising dislocation-engineered silicon light-emitting diodes," *Applied Physics B*, vol. 83, pp. 289–294, 2006. URL: http://dx.doi.org/10.1007/s00340-006-2149-6

[25] B. Burton and M. V. Speight, "The coarsening and annihilation kinetics of dislocation loop," *Philosophical Magazine A*, vol. 53, no. 3, pp. 385–402, 1986. URL: http://dx.doi.org/10.1080/01418618608242839

[26] J. Liu, M. Law, and K. Jones, "Evolution of dislocation loops in silicon in an inert ambient I," *Solid-State Electronics*, vol. 38, no. 7, pp. 1305–1312, 1995. URL: http://dx.doi.org/10.1016/0038-1101(94)00257-G

[27] F. Cristiano, J. Grisolia, B. Colombeau, M. Omri, B. de Mauduit, A. Claverie, L. F. Giles, and N. E. B. Cowern, "Formation energies and relative stability of perfect and faulted dislocation loops in silicon," *Journal of Applied Physics*, vol. 87, no. 12, pp. 8420–8428, 2000. URL: http://dx.doi.org/10.1063/1.373557

[28] G. Z. Pan, K. N. Tu, and A. Prussin, "Size-distribution and annealing behavior of end-of-range dislocation loops in silicon-implanted silicon," *Journal of Applied Physics*, vol. 81, no. 1, pp. 78–84, 1997. URL: http://dx.doi.org/10.1063/1.364099

[29] D. J. Stowe, "An investigation of efficient room temperature luminescence from silicon which contains dislocations," Ph.D. dissertation, University of Oxford, 2006. URL: http://ora.ox.ac.uk/resolve/info:fedora/uuid:9ee073b7-9e3c-4637-9ce1-62e9e4ade69d/THESIS01

[30] M. Sztucki, T. H. Metzger, I. Kegel, A. Tilke, J. L. Rouvière, D. Lübbert, J. Arthur, and J. R. Patel, "X-ray analysis of temperature induced defect structures in boron implanted silicon," *Journal of Applied Physics*, vol. 92, no. 7, pp. 3694–3703, 2002. URL: http://dx.doi.org/10.1063/1.1505982

[31] K. S. Jones, S. Prussin, and E. R. Weber, "A systematic analysis of defects in ion-implanted silicon," *Applied Physics A: Materials Science And Processing*, vol. 45, pp. 1–34, 1988. URL: http://dx.doi.org/10.1007/BF00618760

[32] J. J. Comer, "Electron microscope study of stackingfault formation in boron implanted silicon," *Radiation Effects*, vol. 36, no. 1-2, pp. 57–61, 1978. URL: http://dx.doi.org/10.1080/00337577808233171

[33] Y. L. Huang, M. Seibt, and B. Plikat, "Nonconservative Ostwald ripening of dislocation loops in silicon," *Applied Physics Letters*, vol. 73, no. 20, pp. 2956–2958, 1998. URL: http://dx.doi.org/10.1063/1.122642

[34] M. Milosavljević, G. Shao, M. A. Lourenco, R. M. Gwilliam, and K. P. Homewood, "Engineering of boron-induced dislocation loops for efficient room-temperature silicon light-emitting diodes," *Journal of Applied Physics*, vol. 97, no. 7, p. 073512, 2005. URL: http://dx.doi.org/10.1063/1.1866492

[35] D. Hull and D. J. Bacon, *Introduction to Dislocations*, 5th ed. Amsterdam: Butterworth-Heinemann, 2011.

[36] G. Schoeck and W. A. Tiller, "On dislocation formation by vacancy condensation," *Philosophical Magazine*, vol. 5, no. 49, pp. 43–63, 1960. URL: http://dx.doi.org/10.1080/14786436008241199

[37] N. Martsinovich, "Theory of defects arising from hydrogen in silicon and diamond," Ph.D. dissertation, University of Sussex, 2004. URL: http://www.lifesci.sussex.ac.uk/research/tc/thesis

[38] F. Kroupa, "Circular edge dislocation loop," *Cechoslovackij fiziceskij zurnal B*, vol. 10, pp. 284–293, 1960. URL: http://dx.doi.org/10.1007/BF02033533

[39] R. LeSar, "Ambiguities in the calculation of dislocation self energies," *physica status solidi (b)*, vol. 241, no. 13, pp. 2875–2880, 2004. URL: http://dx.doi.org/10.1002/pssb.200302054

[40] D. J. Bacon and A. G. Crocker, "The elastic energies of symmetrical dislocation loops," *Philosophical Magazine*, vol. 12, no. 115, pp. 195–198, 1965. URL: http://dx.doi.org/10.1080/14786436508224960

[41] W. Cai and C. R. Weinberger, "Energy of a prismatic dislocation loop in an elastic cylinder," *Mathematics and*

Mechanics of Solids, vol. 14, no. 1-2, pp. 192–206, 2009. URL: http://dx.doi.org/10.1177/1081286508092611

[42] C. D. Meekison, "A model of diffusion-controlled annealing of dislocation loops in pre-amorphized silicon," *Philosophical Magazine A*, vol. 69, no. 2, pp. 379–396, 1994. URL: http://dx.doi.org/10.1080/01418619408244350

[43] H. Föll, *Defects in Crystals*. Germany: Lecture Notes, University of Kiel, 2012. URL: http://www.tf.uni-kiel.de/matwis/amat/def_en/

[44] D. B. Holt and B. G. Yacobi, *Extended Defects in Semiconductors — Electronic Properties, Device Effects and Structures*, 1st ed. Cambridge: Cambridge University Press, 2007.

[45] C. Bonafos, A. Martinez, M. Faye, C. Bergaud, D. Mathiot, and A. Claverie, "Transient enhanced diffusion of dopant in preamorphised Si: The role of EOR defects," *Nuclear Instruments and Methods in Physics Research Section B*, vol. 106, no. 1-4, pp. 222–226, 1995. URL: http://dx.doi.org/10.1016/0168-583X(95)00707-5

[46] I. Lifshitz and V. Slyozov, "The kinetics of precipitation from supersaturated solid solutions," *Journal of Physics and Chemistry of Solids*, vol. 19, no. 1-2, pp. 35–50, 1961. URL: http://dx.doi.org/10.1016/0022-3697(61)90054-3

F. Alexander Wolf obtained a M. Sc. in Physics in 2011 from the University of Augsburg. At the time of this work, he was a PhD student at Bosch Corporate Research, Gerlingen, Germany. He now is with the Ludwigs-Maximilians-Universität (LMU), Munich.

Alberto Martinez-Limia obtained his diploma in Nuclear Physics in 1994 from the Institute of Nuclear Sciences and Technology of Havana and his PhD in 2002 from the Institute of Theoretical Chemistry of the University of Erlangen-Nuremberg. Later he worked in several academic and scientific organizations: the University of South Carolina, the University of Chemnitz and the Fraunhofer Institute IISB in Erlangen. He investigated topics related to material modeling and process simulation. In October 2008 he joined the Robert Bosch GmbH as a Research and Development scientist.

Daniel Stichtenoth studied physics at the University of Göttingen, Germany and Uppsala, Sweden. He received his diploma degree in physics in 2005 and his Dr. rer nat in 2008 from the University of Göttingen, Germany. Since 2009 he is with BOSCH Solar Energy AG, Arnstadt, Germany and works in the field of silicon solar cell development. His main focus is on the interaction of silicon with high-efficiency silicon solar cell processes.

Peter Pichler obtained the Dip.-Ing. degree in Electrical Engineering in 1982 and the Dr. techn. degree 1985 both from the Technical University of Vienna. Since 1986 he has been Group Manager at Fraunhofer IISB, responsible now for the doping and device simulation activities. In 2004 he obtained the venia legendis from the University of Erlangen-Nuremberg. Dr. Pichler contributed to various European projects. coordinated the EC projects RAPID, FRENDTECH, and ATOMICS on diffusion and activation phenomena in silicon and silicon-based materials, and coordinates the ICT Project ATEMOX on the modeling of leakage currents and technologies for low-leakage ultrashallow junctions. He is the author or coauthor of some 120 publications in international journals and conference proceedings, and author of the book "Intrinsic Point Defects, Impurities, and Their Diffusion in Silicon" published by Springer Wien-New York.